

A comparison between two fast sweeping algorithms for solving the attenuating VTI eikonal equation

Qi Hao, Umair bin Waheed, KFUPM; Tariq Alkhalifah, KAUST*

SUMMARY

Attenuating transverse isotropy with a vertical symmetry axis (VTI) can be used to determine the directional variation of the wave attenuation in finely layered structures. Specially, complex-valued traveltimes can be used in absorption compensation, imaging and Q tomography etc. The acoustic attenuating VTI eikonal equation governs the complex-valued traveltimes of P-waves in such a medium, whereas the real and imaginary parts of the traveltimes describes the wave phase behavior and its energy absorption, respectively. We use perturbation theory to design two fast sweeping algorithms for solving the acoustic attenuating VTI eikonal equation. Through numerical tests, we study the accuracy and robustness of these algorithms. We find that the algorithm corresponding to the perturbation formulation using only the attenuation parameters is more robust and provides a stable solution compared to the algorithm developed by perturbing both anellipticity and anisotropy parameters. The lessons learned here are vital in the effort to develop a stable algorithm for eikonal equations corresponding to attenuating anisotropic media.

INTRODUCTION

In fluid-filled reservoirs, seismic attenuation is an important component in the accurate description of wave propagation. The horizontal layering combined with fluid content in reservoirs often cause attenuation anisotropy. Laboratory and field observations confirm that wave propagation in reservoir rocks exhibit attenuation anisotropy (Behura et al., 2012; Zhubayev et al., 2015). Attenuating transversely isotropic media with a vertical symmetry axis (VTI) can be used to describe wave attenuation in fluid-saturated reservoirs with a fine layered structure.

Numerical computation of complex-valued traveltimes is useful for attenuation compensation, imaging, and tomography in attenuating media. The real and imaginary parts of complex-valued traveltimes describe the phase of a wave and the amplitude decay due to energy absorption, respectively. The complex-valued eikonal equation governs such traveltimes. However, there is a lack of efficient and accurate algorithms to directly solve the complex-valued eikonal equation, even for a heterogeneous attenuating isotropic medium. This is mainly due to the fact that the existing algorithms developed for the real-valued eikonal equations, such as fast marching and fast sweeping methods, cannot be directly extended to solve the complex-valued eikonal equation (Hao and Alkhalifah, 2017a).

The acoustic attenuating VTI eikonal equation is classified mathematically as a complex-valued coefficient nonlinear differential equation. The existence of the fourth-order term increases the difficulty of solving the acoustic attenuating VTI eikonal equation. Here, we study two potential fast sweep-

ing algorithms to directly solve the acoustic attenuating VTI eikonal equation (Hao and Alkhalifah, 2017a). The two algorithms differ in their perturbation formulation.

The first algorithm requires two perturbation parameters associated with attenuation and anellipticity, which allows us to split the attenuating eikonal equation into a non-attenuating elliptically isotropic eikonal equation, which we can solve easily, and the first- and second-order perturbation equations. The second algorithm requires only one perturbation parameter associated with attenuation, and the acoustic attenuating VTI eikonal equation is split into the non-attenuating VTI eikonal equation and a first-order perturbation term. We present numerical tests to study the accuracy and robustness of these two formulations.

THEORY

The acoustic attenuating VTI eikonal equation is given by (Hao and Alkhalifah, 2017a)

$$At_x^2 + Bt_z^2 + Ct_x^2 t_z^2 = 1, \quad (1)$$

with

$$\begin{aligned} A &= v_x^2 [1 - 2ik_Q(1 + \varepsilon_Q)], \quad B = v_z^2 (1 - 2ik_Q), \\ C &= \frac{v_z^2}{v_x^2(1+2\eta)} \left[(1 - 2ik_Q)v_x^2 - ik_Q\delta_Q v_z^2(1+2\eta) \right]^2 \\ &\quad - v_z^2 v_x^2 (1 - 2ik_Q) [1 - 2ik_Q(1 + \varepsilon_Q)], \\ k_Q &= \frac{A_{P0}}{1 - A_{P0}^2}. \end{aligned}$$

Here t represents the complex traveltime, while t_x and t_z are its spatial derivatives. We use i to denote the imaginary unit, whereas v_z and v_x denote the P-wave vertical and horizontal velocities in the non-attenuating VTI reference medium, respectively. The anellipticity parameter in the non-attenuating VTI reference medium is denoted by η , while A_{P0} denotes the wavenumber-normalized attenuation coefficient of the vertically propagating P-wave. For brevity sake, we refer to the wavenumber-normalized attenuation coefficient as the attenuation coefficient throughout the rest of this expanded abstract. The attenuation-anisotropy parameter describing the fractional difference between the horizontal and the vertical attenuation coefficients is denoted by ε_Q , while the attenuation-anisotropy parameter controlling the curvature of the P-wave attenuation coefficient curve in the vertical direction is denoted by δ_Q .

ALGORITHM 1

In this section, we develop the first perturbation formulation based on two perturbation parameters associated with attenuation and anellipticity. We then propose a fast-sweeping algorithm to efficiently solve the resulting formulation.

Fast sweeping algorithms in attenuating VTI media

In equation 1, let us introduce a dimensionless parameter ζ_1 to replace i and scale k_Q , and a dimensionless parameter ζ_2 to scale η . This leads to the following equation:

$$A_1 t_{,x}^2 + B_1 t_{,z}^2 + C_1 t_{,x}^2 t_{,z}^2 = 1, \quad (2)$$

with

$$\begin{aligned} A_1 &= v_x^2 [1 - 2\zeta_1 k_Q (1 + \varepsilon_Q)], \quad B_1 = v_z^2 (1 - 2\zeta_1 k_Q), \\ C_1 &= \frac{v_z^2}{v_x^2 (1 + 2\zeta_2 \eta)} \left[(1 - 2\zeta_1 k_Q) v_x^2 - \zeta_1 k_Q \delta_Q v_z^2 (1 + 2\zeta_2 \eta) \right]^2 \\ &\quad - v_z^2 v_x^2 (1 - 2\zeta_1 k_Q) [1 - 2\zeta_1 k_Q (1 + \varepsilon_Q)]. \end{aligned}$$

Setting $\zeta_1 = i$ and $\zeta_2 = 1$, equation 2 reduces to the acoustic attenuating VTI eikonal equation. We define the second-order trial solution of equation 2 as

$$t = t_0 + \sum_{i=1}^2 t_i \zeta_i + \sum_{i \leq j=1}^2 t_{ij} \zeta_i \zeta_j, \quad (3)$$

where t_0 , t_i and t_{ij} denote the zeroth-, first- and second-order traveltime coefficients, respectively.

We substitute the trial solution 3 into equation 2 and then expand the result into a second-order Taylor series with respect to the perturbation parameters. The governing equation for t_0 is found to be

$$v_x^2 t_{0,x}^2 + v_z^2 t_{0,z}^2 = 1. \quad (4)$$

The governing equations for t_i ($i = 1, 2$) are

$$v_x^2 t_{0,x} t_{i,x} + v_y^2 t_{0,y} t_{i,y} + v_z^2 t_{0,z} t_{i,z} = f_i(t_0). \quad (5)$$

The governing equations for t_{ij} ($i \leq j = 1, 2$) are

$$v_x^2 t_{0,x} t_{ij,x} + v_y^2 t_{0,y} t_{ij,y} + v_z^2 t_{0,z} t_{ij,z} = f_{ij}(t_0, t_1, t_2). \quad (6)$$

All of these governing equations are real-valued. Once we obtain these travelttime coefficients, we may set $\zeta_1 = i$ and $\zeta_2 = 1$ in equation 3 to obtain the second-order perturbation solution of the acoustic attenuating VTI eikonal equation. Referring to Hao and Alkhalifah (2017b), Shanks transform with respect to ζ_2 accelerates the convergence of the second-order perturbation solution (equation 3). We take the Shanks transform of equation 3 with respect to ζ_2 and then set $\zeta_1 = i$ and $\zeta_2 = 1$. Finally, we obtain the Shanks transform solution:

$$t = t_0 - t_{11} + it_1 + \frac{(t_2 + it_{12})^2}{t_2 + it_{12} - t_{22}}. \quad (7)$$

We use the fast sweeping method with multiplicative factorization (Waheed and Alkhalifah, 2017) to solve equation 4. We decompose the zeroth-order travelttime coefficient t_0 into

$$t_0 = \kappa \tau, \quad (8)$$

such that equation 4 is rewritten as

$$v_x^2 (\kappa_{,x} \tau + \kappa \tau_{,x})^2 + v_z^2 (\kappa_{,z} \tau + \kappa \tau_{,z})^2 = 1. \quad (9)$$

The zeroth-order travelttime factor κ is calculated using the reference medium parameters at the source position (x_0, z_0) ,

$$\kappa = \sqrt{\frac{(x - x_0)^2}{v_x^2(x_0, z_0)} + \frac{(z - z_0)^2}{v_z^2(x_0, z_0)}}, \quad (10)$$

The procedure of Algorithm 1 is as follows:

STEP 1: Discretize $\tau_{,x}$ and $\tau_{,z}$ in equation 9 as

$$\tau_{,x} = \left(\frac{\tau(m,n) - \tau_x}{\Delta x} \right) s_x, \quad \tau_{,z} = \left(\frac{\tau(m,n) - \tau_z}{\Delta z} \right) s_z, \quad (11)$$

where $m = 1, 2, \dots, M$ and $n = 1, 2, \dots, N$ denote the grid indices along the x - and z -directions, respectively. The grid spacings along the x - and z -directions are denoted by Δx and Δz , respectively. s_x and s_z denote the sign variables along the x - and z -directions. $\tau(m,n)$ denotes the unknown zeroth-order travelttime factor at the grid point (m,n) . τ_x and τ_z denote the zeroth-order travelttime factors at the selected neighboring grid points along the x - and z -directions. τ_x and s_x are given by

$$\tau_x = \begin{cases} \tau(m+1,n), & \text{if } t_0(m+1,n) < t_0(m-1,n) \\ \tau(m-1,n), & \text{otherwise} \end{cases}, \quad (12)$$

$$s_x = \begin{cases} -1, & \text{if } \tau_x = \tau(m+1,n) \\ +1, & \text{if } \tau_x = \tau(m-1,n) \end{cases}. \quad (13)$$

τ_z and s_z can be obtain by analogy with the above equations.

We discretize $t_{i,x}$ in equation 5 as

$$t_{i,x} = \left(\frac{t_i(m,n) - t_{ix}}{\Delta x} \right) s_x, \quad (14)$$

with

$$t_{ix} = \begin{cases} t_i(m+1,n), & \text{if } \tau_x(m,n) = \tau(m+1,n) \\ t_i(m-1,n), & \text{if } \tau_x(m,n) = \tau(m-1,n) \end{cases}. \quad (15)$$

The derivatives $t_{i,z}$ in equation 5 and $t_{ij,x}$ and $t_{ij,z}$ in equations 6 are discretized similarly.

STEP 2: Use equation 10 to initialize κ in the whole computational domain. Set the value of τ at the source location to one and its value at the rest of the computational domain to a very large positive value. Set the values of τ_i and τ_{ij} to zero in the whole computational domain. Use equation 8 to calculate t_0 .

STEP 3: Except for the grid point where the source is located, take into account the following four sweeping orders:

$$\begin{aligned} (1) \quad m &= 1 : M, n = 1 : N, & (2) \quad m &= 1 : M, n = N : 1, \\ (3) \quad m &= M : 1, n = 1 : N, & (4) \quad m &= M : 1, n = N : 1, \end{aligned} \quad (16)$$

to solve equations 11, 5 and 6 for all other grid points. For a considered grid point in each of the above orders, we perform the following sub-steps: (1) Solve equation 9 and store its solution to $[\tau]$. (2) Substitute $[\tau]$ and κ into equation 8 and store the result to $[t_0]$. (3) If $[t_0]$ satisfies the minimum travelttime criterion ($[t_0] < t_0$) and the causality condition (see the Appendix of Waheed et al. (2015)), then we will set $t_0 = [t_0]$ and continue with (4); otherwise we will move to the next grid point and start with (1). (4) Calculate $t_{0,x}$ and $t_{0,z}$, solve equation 5 and store its solution to t_i . (5) Calculate $t_{i,x}$ and $t_{i,z}$, solve equation 6 and store its solution to t_{ij} .

STEP 4: If the difference between the estimated t_0 from two consecutive iterations is small enough, stop the iteration, calculate equation 7 and output the result; otherwise continue with step 3.

Fast sweeping algorithms in attenuating VTI media

ALGORITHM 2

In this section, we describe the second perturbation formulation. It requires a single perturbation parameter associated with attenuation. We then can describe another fast sweeping algorithm to implement this perturbation formulation.

Here, we take into account a perturbation parameter ξ . We use ξ to replace i in the eikonal equation 1 and obtain

$$A_2 t_{,x}^2 + B_2 t_{,z}^2 + C_2 t_{,x}^2 t_{,z}^2 = 1, \quad (17)$$

with

$$\begin{aligned} A_2 &= v_x^2 [1 - 2\xi k_Q (1 + \epsilon_Q)], \quad B_2 = v_z^2 (1 - 2\xi k_Q), \\ C_2 &= \frac{v_z^2}{v_x^2 (1 + 2\eta)} [(1 - 2\xi k_Q) v_x^2 - \xi k_Q \delta_Q v_z^2 (1 + 2\eta)]^2 \\ &\quad - v_z^2 v_x^2 (1 - 2\xi k_Q) [1 - 2\xi k_Q (1 + \epsilon_Q)]. \end{aligned}$$

We define the trial solution of equation 17 as

$$t = \tilde{t}_0 + \tilde{t}_1 \xi. \quad (18)$$

Substituting equation 18 into equation 17, and expanding the result with respect to ξ up to the first order, we may obtain the following governing equations for \tilde{t}_0 and \tilde{t}_1 :

$$v_x^2 \tilde{t}_{0,x}^2 + v_z^2 \tilde{t}_{0,z}^2 = 1 + \tilde{f}_0(\tilde{t}_0), \quad (19)$$

$$v_x^2 \tilde{t}_{0,x} \tilde{t}_{1,x} + v_z^2 \tilde{t}_{0,z} \tilde{t}_{1,z} = \tilde{f}_1(\tilde{t}_0), \quad (20)$$

where \tilde{f}_0 and \tilde{f}_1 are real-valued functions. Once the solutions of equations 19 and 20 are known, we may set $\xi = i$ in equation 18 to obtain the approximate eikonal solution:

$$t = \tilde{t}_0 + i\tilde{t}_1. \quad (21)$$

Similar to the first scheme, we decompose \tilde{t}_0 into

$$\tilde{t}_0 = \kappa \tilde{\tau}, \quad (22)$$

and hence equation 19 is rewritten as

$$v_x^2 (\kappa \tilde{\tau}_{,x} + \kappa_{,x} \tilde{\tau})^2 + v_z^2 (\kappa \tilde{\tau}_{,z} + \kappa_{,z} \tilde{\tau})^2 = F(\tilde{\tau}), \quad (23)$$

where κ is given by equation 8 and F is given by

$$F(\tilde{\tau}) = 1 + \tilde{f}_0(\kappa \tilde{\tau}). \quad (24)$$

The numerical procedure for this case is given below:

STEP 1: Discretize $\tilde{\tau}_{,x}$ and $\tilde{\tau}_{,z}$ in equation 23 similar to equations 11, while $\tilde{t}_{1,x}$ and $\tilde{t}_{1,z}$ are analogous to equations 14 and 15.

STEP 2: Use equation 10 to initialize κ and calculate $\kappa_{,x}$ and $\kappa_{,z}$ in the whole computational domain. Set the value of $\tilde{\tau}$ at the source location to 1 and its value at the rest of the computational domain to a very large positive number. Set the values of \tilde{t}_i and \tilde{t}_{ij} to zero in the whole computational domain.

STEP 3: In the whole computational domain, set $F(\tilde{\tau}) = 1$ and use equation 22 to calculate \tilde{t}_0 .

STEP 4: Except for the grid point where the source is located, utilize equation 16 to sweep all other grid points in orders. For

a considered point in the sweeping, we perform the following sub-steps: (1) Solve equation 23 and store its solution to $[\tilde{\tau}]$. (2) Substitute $[\tilde{\tau}]$ and κ into equation 22, and store the result to $[\tilde{t}_0]$. (3) If $[\tilde{t}_0]$ satisfies the minimum traveltimes criterion ($[\tilde{t}_0] < \tilde{t}_0$) and the causality condition (see the Appendix of Waheed et al. (2015)), then we will set $\tilde{t}_0 = [\tilde{t}_0]$ and continue with (4); otherwise we will move to the next grid point and start with (1). (4) Calculate $\tilde{t}_{0,x}$ and $\tilde{t}_{0,z}$, solve equation 20, and store its solution to \tilde{t}_1 .

STEP 5: If the difference between the estimated $\tilde{\tau}$ from two consecutive iteration is small enough, then continue with step 6; otherwise, repeat step 4.

STEP 6: Use equation 24 to calculate the function F in the whole computational domain. If the difference between the estimated F from two consecutive results is small enough, then stop and output $t = \tilde{t}_0 + i\tilde{t}_1$; otherwise perform step 4.

NUMERICAL EXAMPLES

Here we compare the accuracy and robustness of the two algorithms discussed above. First, we consider a homogeneous acoustic attenuating VTI model with strong attenuation and moderate attenuation anisotropy. The model parameters include $v_z = 3.0$ km/s, $v_x = 3.349$ km/s, $\eta = 0.167$, $A_{P0} = 0.02498$ (corresponding to $Q_{33} = 20$), $\epsilon_Q = 0.25$, $\delta_Q = 0.4$. For benchmarking, we calculate the exact traveltimes for a homogeneous attenuating anisotropic medium using the work of Vavryčuk (2007). Figure 1 shows the real and imaginary parts of the exact traveltimes solution. Figures 2 and 3 plot the traveltime errors corresponding to Algorithm 1 and 2, respectively. A comparison between Figures 2 and 3 illustrates that for the real part of the traveltimes, as expected Algorithm 2 is more accurate but for the imaginary part of the traveltimes, Algorithm 1 has better accuracy. Nevertheless, traveltime errors in both cases are negligible for most practical purposes. Next, we test the stability of the two algorithms using a complex model such as the attenuating VTI Marmousi model (Figure 4). As illustrated, the model has sharp discontinuities and therefore constitutes a stiff test of robustness for both algorithms. We plot the traveltime solutions using Algorithm 1 and 2 in Figures 5 and 6, respectively. It is obvious that Algorithm 1 suffers from numerical artifacts (due to the perturbation associated with η in the heterogeneous case) but Algorithm 2 provides a stable solution and do not suffer from such artifacts.

CONCLUSIONS

We develop two fast sweeping algorithms to solve the attenuating VTI eikonal equation. We show that both algorithms are sufficiently accurate for a homogeneous attenuating VTI model. However, Algorithm 2, which is based on perturbation formulation using only the attenuation parameter, is more robust for realistic models but more costly in computation. Algorithm 2 can be extended to attenuating anisotropic media with lower symmetry. It can also be further developed to admit Gaussian beams for acoustic imaging in attenuating anisotropic media.

Fast sweeping algorithms in attenuating VTI media

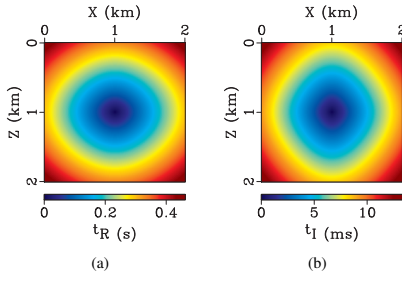


Figure 1: The real and imaginary parts of the exact traveltimes. The source is located at $x = 1$ km and $z = 1$ km.

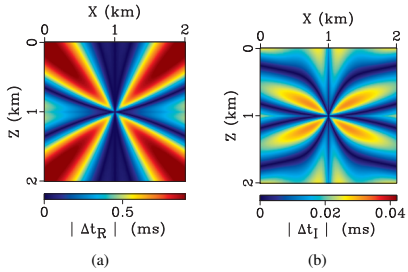


Figure 2: Traveltimes errors in the real (a) and imaginary (b) parts computed using Algorithm 1.

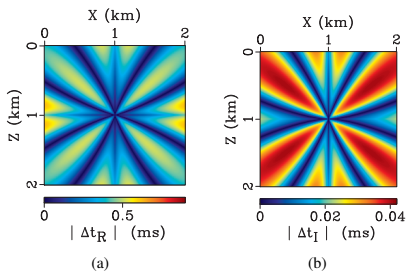


Figure 3: Traveltimes errors in the real (a) and imaginary (b) parts computed using Algorithm 2.

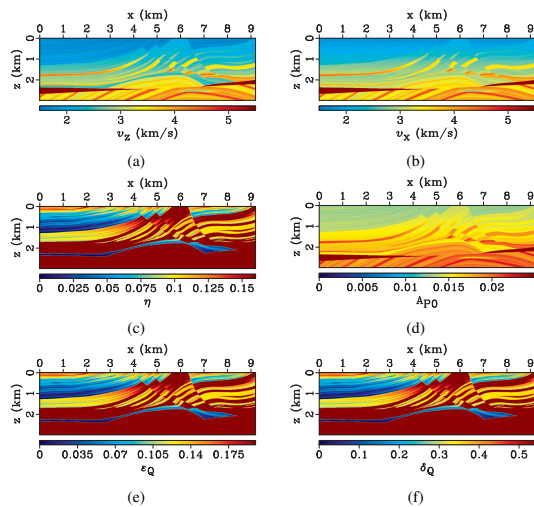


Figure 4: The attenuating VTI Marmousi model with sharp discontinuities.

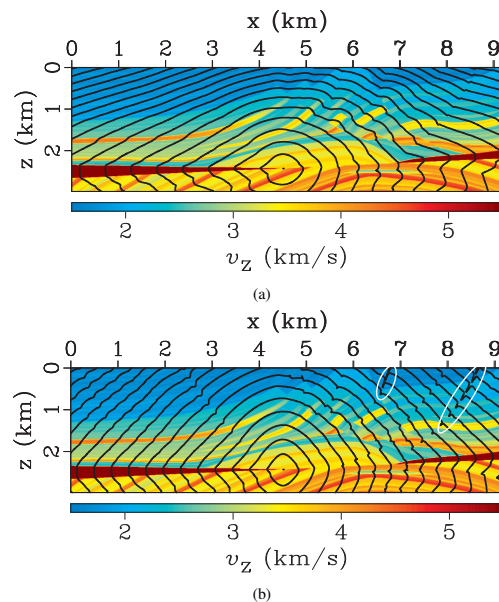


Figure 5: The contours of the real (a) and imaginary (b) parts of the traveltimes in the considered Marmousi model computed using Algorithm 1. The source is located at $x = 4.5$ km and $z = 2.43$ km. The time intervals of two neighboring contour lines are 0.1s (a) and 2ms (b). The white ellipses in plot (b) highlight the numerical artifacts in the imaginary part of the traveltime solution.

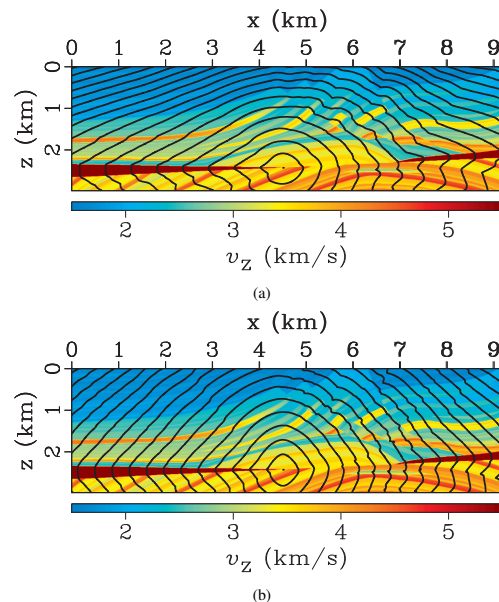


Figure 6: The contours of the real (a) and imaginary (b) parts of the traveltimes in the considered Marmousi model computed using Algorithm 2. The source is located at $x = 4.5$ km and $z = 2.43$ km. The time intervals of two neighboring contour lines are 0.1s (a) and 2ms (b). The imaginary part of the traveltime solution is free from numerical artifacts.

REFERENCES

- Behura, J., I. Tsvankin, E. Jenner, and A. Calvert, 2012, Estimation of interval velocity and attenuation anisotropy from reflection data at coronation field: *The Leading Edge*, **31**, 580–587, doi: <https://doi.org/10.1190/tle31050580.1>.
- Hao, Q., and T. Alkhalifah, 2017a, An acoustic eikonal equation for attenuating transversely isotropic media with a vertical symmetry axis: *Geophysics*, **82**, no. 1, C9–C20, doi: <https://doi.org/10.1190/geo2016-0160.1>.
- Hao, Q., and T. Alkhalifah, 2017b, Acoustic eikonal solutions for attenuating VTI media: 87th Annual International Meeting, SEG, Expanded Abstracts, 289–293, doi: <https://doi.org/10.1190/segam2017-17661832.1>.
- Vavryčuk, V., 2007, Ray velocity and ray attenuation in homogeneous anisotropic viscoelastic media: *Geophysics*, **72**, no. 6, D119–D127, doi: <https://doi.org/10.1190/1.2768402>.
- Waheed, U. B., and T. Alkhalifah, 2017, A fast sweeping algorithm for accurate solution of the tilted transversely isotropic eikonal equation using factorization: *Geophysics*, **82**, no. 6, WB1–WB8, doi: <https://doi.org/10.1190/geo2016-0712.1>.
- Waheed, U. B., C. E. Yarman, and G. Flagg, 2015, An iterative, fast-sweeping-based eikonal solver for 3D tilted anisotropic media: *Geophysics*, **80**, no. 3, C49–C58, doi: <https://doi.org/10.1190/geo2014-0375.1>.
- Zhubayev, A., M. E. Houben, D. M. J. Smeulders, and A. Barnhoorn, 2015, Ultrasonic velocity and attenuation anisotropy of shales, Whitby, United Kingdom: *Geophysics*, **81**, no. 1, D45–D56, doi: <https://doi.org/10.1190/geo2015-0211.1>.